Active Noise Cancellation for a Three-Dimensional Enclosure by Using Multiple-Channel Adaptive Control and H_∞ Control

M. R. Bai

Z. Lin

Department of Mechanical Engineering,
National Chiao-Tung University,
1001 Ta-Hsueh Rd.,
Hsin-Chu, Taiwan, Republic of China

Active noise control (ANC) techniques for a three-dimensional enclosure are compared in terms of two control structures and two control algorithms. The multiple-channel filtered-x least-mean-square (FXLMS) algorithm and the H_∞ robust control algorithm are employed for controller synthesis. Both feedforward and feedback control structures are compared. The Youla's parameterization is employed in the formulation of the multiple-channel feedback FXLMS algorithm. The algorithms are implemented using a floating-point digital signal processor (DSP). Experiments are carried out to validate the ANC approaches for attenuation of the internal field in a rectangular wooden box. Position and number of actuators and sensors are also investigated. A broadband random noise and an engine noise are chosen as the primary noises in the experiments. The experimental results indicate that the feedforward structure yields a broader band of attenuation than the feedback structure. The FXLMS control and H_∞ control achieve comparable performance.

Introduction

Although Paul Lueg proposed the idea of active noise control (ANC) long before in 1936, the technique did not seem to receive full research attention. It languished until the late 1980's when the conjunction of inexpensive digital signal processors (DSP), adaptive algorithms, and application needs inspired a renaissance in this area. A good review can be found in the paper by Elliott and Nelson (1994). The ANC technique provides a useful alternative to conventional passive means. The advantages of ANC techniques are: improved low-frequency performance, reduction of size and weight, low cost, low back pressure, programmable flexibility of design, and so forth.

In viewing the ANC applications to date, much of the work has focused on cancellation of the plane-wave modes in ducts and small-volume enclosures such as headsets (Elliott and Nelson, 1994), in which case the use of a single-channel controller is sufficient to attenuate the noise field over low-frequency ranges. On the other hand, multiple-channel ANC finds applications in attenuating noise in automobile cabins and aircraft cabins (Nelson and Elliott, 1992; Kuo and Morgan, 1996). However, as compared to duct or headset applications, multiple-channel ANC systems remain less developed for full commercialization. The complexity of multiple-channel ANC stems from the fact that sound fields in large-volume enclosures become three-dimensional in nature and the high-order modes can no longer be disregarded (Kinsler et al., 1982). It is this increased dimensionality of the problem that poses a severe challenge for ANC techniques, especially when broadband attenuation is of interest (Fuller and Von Flotow, 1995). In principle, below the Schroeder's cutoff frequency, it is necessary to distribute as many as possible sensors and actuators in an enclosure to achieve nearly global attenuation (Nelson and Elliott, 1992). As a general guideline, one must avoid positioning the actuators and sensors at the nodal points of the dominant acoustic modes in the enclosure. Minimization of the mean square of the sensor outputs is closely equivalent to the minimization of the global acoustic potential energy (Molo and Bernhard, 1989; Lester and Fuller, 1990; Cunefare and Koopmann, 1991; Elliott et al., 1992; Bai and Chang, 1996).

In this paper, ANC techniques for a three-dimensional enclosure are compared in terms of two control structures and two control algorithms. The well-known multiple-input-multiple-output (MIMO) filtered-x least-mean-square (FXLMS) algorithm and the H_∞ robust control algorithm are employed for controller synthesis. Both feedforward and feedback control structures are compared. The Youla's parameterization is employed in the formulation of the MIMO feedback FXLMS algorithm to assure that the resulting system is internally stable. On the other hand, the H_∞ robust control theory provides a general and unified framework for all control structures and it makes virtually no distinction as to whether the system is single-channel or multiple-channel (Doyle et al., 1989; Yeh and Yang, 1992; Tsai and Tsai, 1995). By choosing appropriate weighting functions, the H_∞ control theory is capable of accommodating simultaneously the requirements of robust performance and robust stability in the face of modeling uncertainties and plant perturbations.

The ANC algorithms are implemented on a floating-point DSP. Experiments are carried out to validate the proposed ANC approaches for attenuation of the internal field in a rectangular wooden box. The effects of position and number of actuators and sensors on the active control are also investigated. A broadband random noise and an engine noise are chosen as the primary noises in the experiments.

Multiple-Channel Adaptive ANC Algorithms

The multiple-channel feedforward and feedback FXLMS algorithms are presented in this section. A general MIMO ANC system using H reference sensors, L secondary sources, and M error sensors is illustrated in Fig. 1(a). $\mathbf{P}(z)$ is the transfer matrix representing the primary paths. $\mathbf{S}(z)$ is the transfer matrix ($M \times L$) of the secondary cancellation paths formed by actuators, acoustic error paths, and error sensors.

First, the MIMO feedforward FXLMS (also known as the multiple-error FXLMS) algorithm is briefly reviewed. More detailed derivations can be found in the literature (Elliott et al.,

Contributed by the Technical Committee on Vibration and Sound for publication in the JOURNAL OF VIBRATION AND ACOUSTICS. Manuscript received June 1997. Associate Technical Editor: R. Clark.

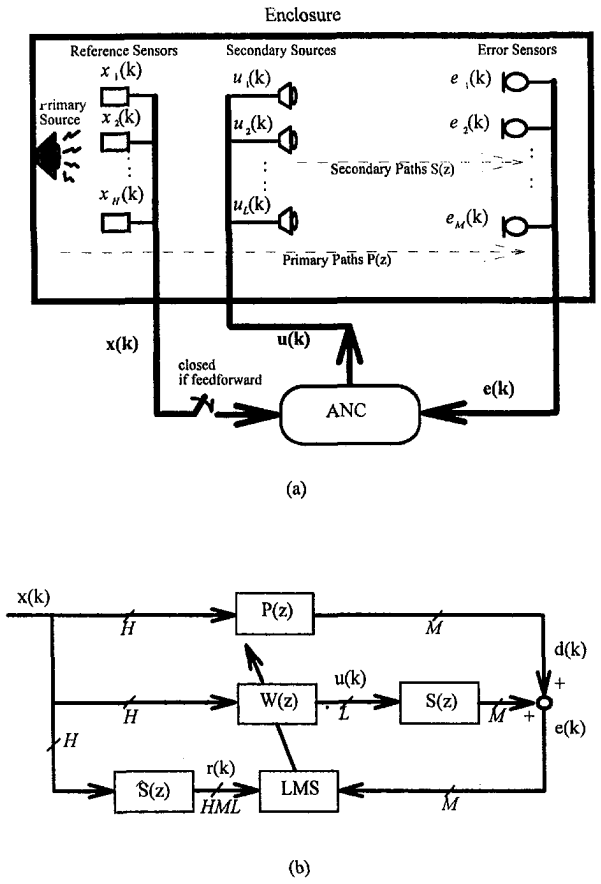

Fig. 1 A multiple-channel ANC problem (*a*) general MIMO ANC system (*b*) block diagram of a MIMO ANC system using the feedforward FXLMS algorithm

1987; Elliott et al., 1992; Snyder and Hansen, 1992). In Fig. 1(*a*), H reference signals, $x_h(k)$, are measured, for simplicity, by H nonacoustical reference sensors. In this study, the voltage signal driving the primary source is used as the reference. The control signals $u_l(k)$ driving the L secondary sources are produced by the MIMO controller that in turn comprises $L \times H$ I-th order FIR filters with coefficients, w_{lhi}. Then the control signals from the controller can be written as

$$u_l(k) = \sum_{h=1}^{H} \sum_{i=0}^{I-1} w_{lhi} x_h(k-i). \quad (1)$$

The secondary paths are modeled as J-th order FIR filters with coefficients, s_{mlj}. The error signal measured by the m-th error sensor can be expressed as

$$e_m(k) = d_m(k) + \sum_{l=1}^{L} \sum_{j=0}^{J} s_{mlj} u_l(k-j), \quad (2)$$

where $d_m(k)$ is the primary noise measured at the m-th error sensor. By the gradient search that seeks to minimize the cost function

$$J(k) = \sum_{m=1}^{M} e_m^2(k), \quad (3)$$

one can obtain the update formula of the filter coefficients

$$w_{lhi}(k+1) = w_{lhi}(k) - \mu \sum_{m=1}^{M} e_m r_{mlh}(k-i), \quad (4)$$

where μ is the convergence factor and $r_{mlh}(k)$ is formed by filtering the h-th reference signal by the secondary-path model from the l-th secondary source to the m-th error sensor, i.e.,

$$r_{mlh}(k) = \sum_{j=0}^{J-1} \hat{s}_{mlj} x_h(k-j). \quad (5)$$

The block diagram of the MIMO feedforward FXLMS algorithm is shown in Fig. 1(*b*), where $\mathbf{u}(k)$ is the control signal vector, $\mathbf{W}(z)$ is the $(H \times L)$ transfer matrix of the FIR controller, $\mathbf{d}(k)$ is the primary noise vector, $\mathbf{e}(k)$ is the error signal vector, and the matrix $\hat{\mathbf{S}}(z)$ represents the estimate of $\mathbf{S}(z)$.

Next, the MIMO feedback FXLMS algorithm is derived. Consider the classical MIMO feedback structure shown in Fig. 2(*a*). The matrix $\mathbf{S}(z)$ is the transfer function of the plant (secondary path). The matrix $\mathbf{S}(z)$ is assumed to be stable, as is generally the case in ANC problems. The matrix $\mathbf{C}(z)$ is the transfer matrix of the MIMO controller. The vector $\mathbf{u}(k)$ is the control signal vector produced by $\mathbf{C}(z)$. By the Youla Parametrization (Youla et al., 1976), the set of controllers Γ that ensures internal stability of the closed-loop system can be expressed as

$$\Gamma = \{\mathbf{W}(z)[\mathbf{I} - \mathbf{S}(z)\mathbf{W}(z)]^{-1} | \mathbf{S}(z), \mathbf{W}(z) \in RH_\infty\}, \quad (6)$$

where RH_∞ denotes the space of all proper and stable real rational transfer matrices. The block diagram of the feedback system containing a stabilizing controller $\mathbf{C}(z) \in \Gamma$ (parametrized by $\mathbf{W}(z)$) is shown in Fig. 2(*b*). With this setup, one can simply choose $\mathbf{W}(z)$ as an $(L \times M)$ FIR filter matrix (which surely $\in RH_\infty$) to ensure the internally stability, and adjust the coefficients of $\mathbf{W}(z)$ via the FXLMS algorithm to minimize the residual noise $\mathbf{e}(k)$. Let the coefficients of the $L \times M$ I-th order FIR filters be w_{lmi}. Then the control signals $u_l(k)$ can be written as

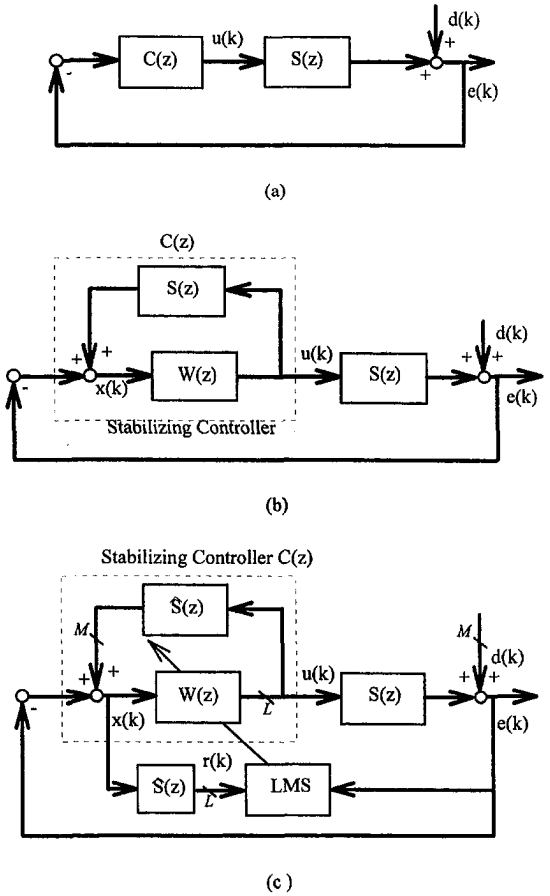

Fig. 2 A multiple-channel feedback ANC problem (*a*) classical feedback ANC system (*b*) block diagram of a feedback system containing a stabilizing controller (*c*) block diagram of a MIMO ANC system using the feedback FXLMS algorithm

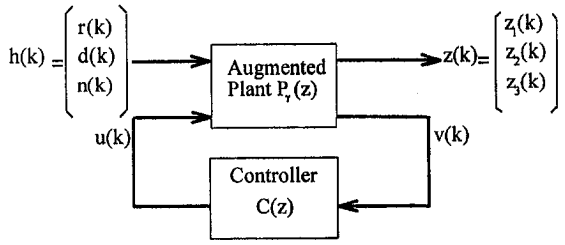

Fig. 3 Generalized control framework

$$u_l(k) = \sum_{m=1}^{M} \sum_{i=0}^{I-1} w_{lmi} x_m(k-i). \tag{7}$$

Note however that the reference signals $x_m(k)$ are not directly measurable and must be synthesized by the following equation:

$$x_m(k) = \sum_{l=1}^{L} \sum_{j=0}^{J} \hat{s}_{mlj} u_l(k-j) - e_m(k), \tag{8}$$

where s_{mlj} is as defined earlier. From Fig. 2(*b*), the residual noise can be expressed as

$$\mathbf{e}(k) = \mathbf{d}(k) + [\mathbf{s}(k) * \mathbf{w}(k)] * \mathbf{x}(k), \tag{9}$$

where $*$ denotes convolution. Similar to the feedforward FXLMS algorithm, it can be shown that minimizing the cost function of Eq. (3) leads to the filter update formula

$$w_{lmi}(k+1) = w_{lmi}(k) - \mu \sum_{h=1}^{M} e_h(k) r_{hlm}(k-i), \tag{10}$$

where

$$r_{hlm}(k) = \sum_{j=0}^{J-1} \hat{s}_{hlj} x_m(k-j) \tag{11}$$

are the filtered synthesized reference signals; $e_h = e_m$ and $\hat{s}_{hlj} = \hat{s}_{mlj}$, for $h = m$.

The architecture of the MIMO feedback FXLMS algorithm is schematically shown in the block diagram of Fig. 2(*c*).

Multiple-Channel H_∞ ANC Algorithms

1. H_∞ Robust Control Theory. The H_∞ theories can be found in much control literature (e.g., Doyle et al., 1989; Iglesias and Glover, 1991; Yeh and Yang, 1992; Tsai and Tsai, 1995) and we present only the key part needed in the development of the ANC algorithms. The rest are mentioned without proof. In our study, since the system model identified by a parametric procedure is in the discrete-time domain, we present only the discrete-time version of the H_∞ algorithm. It is also remarked that the H_∞ algorithms can be divided into two classes (Lin, 1994): the model matching algorithms (the 1984 approach) and the two Riccati equation algorithms (the 1988 approach). We utilize only the latter approach, which does not require a chain of factorizations as in the model matching approach, and thus numerical problems in handling high-order (acoustical) plants can be minimized.

In modern control theory, all control structures can be cast into a generalized control framework, as depicted in Fig. 3. The framework contains a controller $\mathbf{C}(z)$ and an *augmented plant* $\mathbf{P}_\gamma(z)$. The controlled variable $\mathbf{z}(k)$ corresponds to various control objectives $\mathbf{z}_1(k)$, $\mathbf{z}_2(k)$, and the extraneous input $\mathbf{b}(k)$ consists of the reference $\mathbf{r}(k)$, the disturbance $\mathbf{d}(k)$, and the noise $\mathbf{n}(k)$. The signal $\mathbf{u}(k)$ and $\mathbf{v}(k)$ are the control input to the plant and the measured output from the plant, respectively. The general input-output relation can be expressed as

$$\begin{bmatrix} \mathbf{Z}(z) \\ \mathbf{V}(z) \end{bmatrix} = \begin{bmatrix} \mathbf{P}_{11}(z) & \mathbf{P}_{12}(z) \\ \mathbf{P}_{21}(z) & \mathbf{P}_{22}(z) \end{bmatrix} \begin{bmatrix} \mathbf{B}(z) \\ \mathbf{U}(z) \end{bmatrix}$$

$$= \mathbf{P}_\gamma(z) \begin{bmatrix} \mathbf{B}(z) \\ \mathbf{U}(z) \end{bmatrix}, \tag{12}$$

where the submatrices $\mathbf{P}_{ij}(z)$, $i, j = 1, 2$ are compatible partitions of the augmented plant $\mathbf{P}_\gamma(z)$ and the signal variables are capitalized to represent z-domain quntities.

The rationale of the H_∞ control is to minimize the infinity norm of the transfer matrix $\mathbf{T}(z)$ between output $\mathbf{z}(k)$ and the input $\mathbf{b}(k)$

$$\mathbf{T}(z) = \mathbf{P}_{11}(z) + \mathbf{P}_{12}(z)\mathbf{C}(z)[\mathbf{I} - \mathbf{P}_{22}(z)\mathbf{C}(z)]^{-1}\mathbf{P}_{21}(z). \tag{13}$$

This is referred to as the optimal H_∞ problem (Yeh and Yang, 1992):

$$\min_{\mathbf{C}(z)} \|\mathbf{T}(z)\|_\infty, \tag{14}$$

where $\|\mathbf{T}(z)\|_\infty = \sup_{0 \le \theta \le 2\pi} \bar{\sigma}[\mathbf{T}(e^{j\theta})]$ is the infinity norm of the transfer matrix $\mathbf{T}(z)$ and is the maximum energy in the output from the transfer function due to any input of unit energy ($\bar{\sigma}$ denotes the maximum singular value). However, because the optimal solution is generally difficult to obtain, one is content with the suboptimal solution: finding $\mathbf{C}(z)$ such that $\|\mathbf{T}(z)\|_\infty < \gamma$, where γ is a number which one wants to make it as small as possible. The details of the synthesis procedures of the H_∞ controllers per solving the Riccati equations can be found in the paper by Tsai and Tsai (1995) and are thus omitted for brevity.

2 Control Structures. In this section, feedforward and feedback structures are formulated on the basis of the generalized control framework. The feedforward structure is illustrated in Fig. 4(a) in terms of the generalized control framework. $\mathbf{P}(z)$, $\mathbf{S}(z)$, and $\mathbf{C}(z)$ denote the transfer matrices of the primary path, the secondary path, and the MIMO controller, respectively. To find an H_∞ controller, we shall weight the output of the transfer function matrix $\tilde{\mathbf{Q}}(z)$ by $\mathbf{W}_1(z)$, and the control input vector $\mathbf{u}(k)$ by $\mathbf{W}_2(z)$, where

$$\tilde{\mathbf{Q}}(z) = [\mathbf{P}(z) + \mathbf{S}(z)\mathbf{C}(z)]^{-1} \tag{15}$$

is the transfer matrix between the disturbance $\mathbf{d}(k)$ and the residual noise $\mathbf{e}(k)$. Note that of these weighting functions should not be confused with the FIR filter taps used in the FXLMS method. For good disturbance rejection, the nominal performance condition must be satisfied

$$\|\tilde{\mathbf{Q}}(z)\mathbf{W}_1(z)\|_\infty < \gamma. \tag{16}$$

In general, $\mathbf{W}_1(z)$ is chosen to be a lowpass function matrix with desired cutoff. The input-output relation of the augmented plant associated with the feedforward structure is

$$\begin{bmatrix} \mathbf{Z}_1(z) \\ \mathbf{Z}_2(z) \\ \mathbf{V}(z) \end{bmatrix} = \begin{bmatrix} \mathbf{W}_1(z)\mathbf{P}(z) & \mathbf{W}_1(z)\mathbf{S}(z) \\ 0 & \mathbf{W}_2(z) \\ I & 0 \end{bmatrix} \begin{bmatrix} \mathbf{D}(z) \\ \mathbf{U}(z) \end{bmatrix}. \tag{17}$$

Hence, as per Eq. (13), the suboptimal condition of the H_∞ feedforward controller reads

$$\left\| \begin{bmatrix} \mathbf{W}_1(z)[\mathbf{P}(z) + \mathbf{S}(z)\mathbf{C}(z)] \\ \mathbf{W}_2(z)\mathbf{C}(z) \end{bmatrix} \right\|_\infty < \gamma. \tag{18}$$

Next, the feedback structure is illustrated in Fig. 4(*b*) in terms of the generalized control framework. To find an H_∞

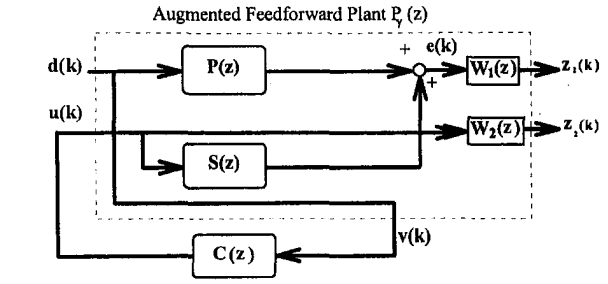

(a)

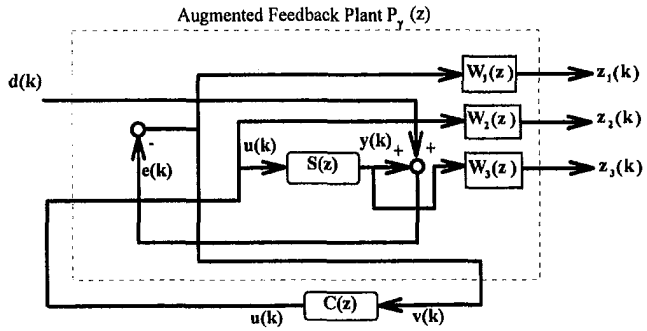

(b)

Fig. 4 ANC structures in terms of the generalized control framework (*a*) feedforward control structure (*b*) feedback control structure

controller, we shall weight the sensitivity matrix $\tilde{\mathbf{S}}(z)$ by $\mathbf{W}_1(z)$, the control input vector $\mathbf{u}(k)$ by $\mathbf{W}_2(z)$, and the complementary sensitivity matrix $\tilde{\mathbf{T}}(z)$ with $\mathbf{W}_3(z)$. The sensitivity matrices $\tilde{\mathbf{S}}(z)$ and $\tilde{\mathbf{T}}(z)$ are the measures of nominal performance and robust stability and are defined as (Doyle et al., 1992)

$$\tilde{\mathbf{S}}(z) = [\mathbf{I} + \mathbf{S}(z)\mathbf{C}(z)]^{-1}, \tag{19}$$

and

$$\tilde{\mathbf{T}}(z) = \mathbf{S}(z)\mathbf{C}(z)[\mathbf{I} + \mathbf{S}(z)\mathbf{C}(z)]^{-1} = \mathbf{S}(z)\mathbf{C}(z)\tilde{\mathbf{S}}(z). \tag{20}$$

For good disturbance rejection and tracking performance, the nominal performance condition must be satisfied

$$\|\tilde{\mathbf{S}}(z)\mathbf{W}_1(z)\|_\infty < \gamma. \tag{21}$$

On the other hand, for system stability against plant perturbations and model uncertainties, the robustness condition (that can be derived from the *small-gain theorem* (Doyle et al., 1992)) must be satisfied

$$\|\tilde{\mathbf{T}}(z)\mathbf{W}_3(z)\|_\infty < \gamma. \tag{22}$$

In general, $\mathbf{W}_1(z)$ is chosen to be a lowpass function matrix, $\mathbf{W}_2(z)$ is chosen to be a small diagonal constant matrix, and $\mathbf{W}_3(z)$ is chosen to be a highpass function matrix. Because $\tilde{\mathbf{S}}(z) + \tilde{\mathbf{T}}(z) = \mathbf{I}$, the tradeoff between $\tilde{\mathbf{S}}(z)$ and $\tilde{\mathbf{T}}(z)$, which is in turn compounded by the *waterbed effect,* severely dictates the performance and robustness of the feedback design. This classical tradeoff renders the following *mixed sensitivity problem* (Yeh and Yang, 1992):

$$\| |\tilde{\mathbf{S}}(z)\mathbf{W}_1(z)| + |\tilde{\mathbf{T}}(z)\mathbf{W}_3(z)| \|_\infty < \gamma. \tag{23}$$

The input-output relation of the augmented plant associated with the feedback structure can be expressed as

$$\begin{bmatrix} \mathbf{Z}_1(z) \\ \mathbf{Z}_2(z) \\ \mathbf{Z}_3(z) \\ \mathbf{V}(z) \end{bmatrix} = \begin{bmatrix} -\mathbf{W}_1(z) & -\mathbf{W}_1(z)\mathbf{S}(z) \\ \mathbf{0} & \mathbf{W}_2(z) \\ \mathbf{0} & \mathbf{W}_3(z)\mathbf{S}(z) \\ -\mathbf{I} & -\mathbf{S}(z) \end{bmatrix} \begin{bmatrix} \mathbf{D}(z) \\ \mathbf{U}(z) \end{bmatrix}. \tag{24}$$

Thus, as per Eq. (13), the suboptimal condition of the feedback controller reads

$$\left\| \begin{bmatrix} \mathbf{W}_1(z)\tilde{\mathbf{S}}(z) \\ \mathbf{W}_2(z)\tilde{\mathbf{R}}(z) \\ \mathbf{W}_3(z)\tilde{\mathbf{T}}(z) \end{bmatrix} \right\|_\infty < \gamma, \tag{25}$$

where

$$\tilde{\mathbf{R}}(z) = \mathbf{C}(z)[\mathbf{I} + \mathbf{S}(z)\mathbf{C}(z)]^{-1} = \mathbf{C}(z)\tilde{\mathbf{S}}(z). \tag{26}$$

The beauty of the H_∞ lies in the fact that there is essentially no difference between the procedures of how one obtains the feedback controller and the feedforward controller, except the augmented matrices in Eqs. (17) and (24) are different.

Experimental Investigations

1. Experimental Arrangement. The three-dimensional enclosure used for the experiments is a rectangular wooden box with width 0.7 m, height 0.8 m, and depth 0.9 m, as shown in Fig. 5. The Schroeder's cutoff frequency of the box is approximately 563 Hz, and thus our control bandwidth is targeted at 50 ~ 400 Hz. The primary noise source is mounted at the center of the far-side wall. The secondary sources L_1 and L_2 are mounted at the centers of the opposite side walls. The secondary sources L_3 and L_4 are mounted at the kitty corners of the near-side wall. The error sensors M_1, M_2, M_3, and M_4 are collocated with the secondary sources L_1, L_2, L_3, and L_4, respectively. The voltage signal of the primary source is used as the reference signal. The algorithms are implemented on a 32-bit floating-point DSP (TMS320C31) in conjunction with a four-channel analog I/O module. The sampling rate is selected to be 2 kHz. Prior to designing the controllers, the models of the primary path $\mathbf{P}(z)$ and the secondary path $\mathbf{S}(z)$ were determined using a parametric ARX system identification procedure (Ljung, 1987). After the models are obtained, the *balanced truncation* technique (McFarlane and Glover, 1989) is applied to reduce the

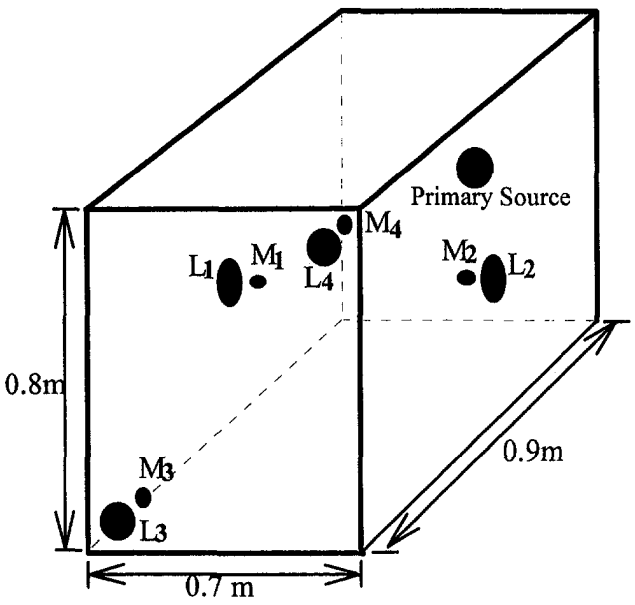

Fig. 5 A schematic diagram of the enclosure used in the experiments

Table 1 The order-reduced models of the primary paths identified by the ARX procedure, where *P* stands for the primary plant; the subsripts 3 and 4 stand for the corresponding microphone numbers.

$P_3(z)$		$P_4(z)$	
zeros	poles	zeros	poles
-6.6131	-0.9595	-4.3696	-0.8442
0.0755±4.4316i	-0.5775±0.2500i	0.5570±2.9807i	-0.7478±0.3597i
-1.9451	-0.4988±0.4193i	-2.2667	0.2091±0.8316i
2.7052	0.4243±0.8280i	2.6196	0.7018±0.7008i
-0.9809	0.7125±0.6900i	1.4692	0.7545±0.6463i
1.5131	0.7498±0.6016i	0.7403±0.7110i	0.8357±0.5440i
0.3347±0.7854i	0.8172±0.5384i	0.7536±0.6615i	0.8114±0.4929i
0.7090±0.6811i	0.8731±0.4111i	0.8361±0.5424i	0.8914±0.4165i
0.8024±0.6453i	0.9509±0.2853i	0.8082±0.4397i	0.9557±0.2769i
0.8055±0.5177i	0.9940±0.0776i	0.9507±0.2558i	0.9953±0.0823i
0.9409±0.2763i	0.9714±0.1232i	0.9900±0.0761i	0.9672±0.1297i
0.9936±0.0356i		0.9975	
0.9077±0.0554i		0.2623±0.0701i	
gain = -4.4102E-5		gain = -1.0322E-4	

orders of the models during controller design. Tables 1 and 2 give examples of the order-reduced models of the primary path and the secondary path identified by the ARX procedure.

2. Experimental Results and Discussions. In the following experimental cases, several performance indices are employed to facilitate the performance comparison of the ANC methods. First, the sum of the power spectra of the error signals is defined as (global energy)

$$\hat{E}_g(f) = \sum_{m=1}^{4} \hat{E}_m(f), \tag{27}$$

where $\hat{E}_m(f)$ denotes the power spectrum of the residual field measured at the m-th error sensor as a function of the frequency f. Then, a performance index ATT_g (global attenuation) intended for measuring the global control performance is defined as the total attenuation of $\hat{E}_g(f)$ over the control bandwidth (50 ~ 400 Hz)

$$ATT_g = 10 \cdot \log \left(\int_{50}^{400} \hat{E}_{gu}(f)df \Big/ \int_{50}^{400} \hat{E}_{gc}(f)df \right), \tag{28}$$

where the subscripts "u" and "c" stand for "uncontrolled" and "controlled", respectively. Third, a performance index ATT_m intended for measuring local control performance at the m-th error sensor is defined as the total attenuation of $\hat{E}_m(f)$ over the control bandwidth 50 ~ 400 Hz

$$ATT_m = 10 \cdot \log \left(\int_{50}^{400} \hat{E}_{mu}(f)df \Big/ \int_{50}^{400} \hat{E}_{mc}(f)df \right). \tag{29}$$

Table 2 The order-reduced models of the secondary paths identified by the ARX procedure, where *S* stands for the secondary plant; the subscripts correspond to the speaker input and the microphone output.

$S_{33}(z)$		$S_{34}(z)$	
zeros	poles	zeros	poles
0.4446±2.8553i	-0.7504	0.4309±1.1801i	0.2663±0.9343i
-1.9213	-0.3649±0.4738i	0.1614±0.9442i	0.4087±0.8352i
2.8366	0.7944±0.5692i	1.0097±1.0384i	0.5985±0.7223i
-1.0335	0.9153±0.1683i	1.5489±0.0966i	0.7512±0.6263i
0.7840±0.5598i	0.2846±0.4718i	0.7270±0.6215i	0.8343±0.5337i
1.0459		0.9173±0.5035i	0.9548±0.2711i
0.8761		0.9245±0.2903i	0.9826±0.1079i
		1.0343±0.0326i	0.9049±0.1600i
gain = -1.12E-2		gain = -2E-3	

$S_{43}(z)$		$S_{44}(z)$	
zeros	poles	zeros	poles
-15.8595	0.3180±0.9090i	0.4133±2.5893i	-0.8905
-1.4986	0.5061±0.7822i	-1.6120	-0.4437±0.5089i
0.3562±1.2103i	0.6300±0.7456i	2.6196	0.2622±0.6099i
1.0199±0.8929i	0.7548±0.6284i	-1.0174	0.8216±0.5409i
0.6387±0.6870i	0.8314±0.5443i	0.8246±0.5325i	0.9775±0.1325i
0.7990±0.5805i	0.9589±0.2676i	0.9691±0.1142i	0.8423±0.2204i
0.9007±0.3143i	0.9881±0.1122i	1.0363	
1.0868±0.1158i	0.9696±0.1769i	0.4521	
0.9516±0.0806i			
gain = 7.5349E-5		gain = -1.92E-2	

Table 3 Experiment cases (Part 1). The effects of number and position of sensors and actuators on ANC are investigated using the feedforward FXLMS algorithm.

Primary noise: band-limited (0~400 Hz) random noise.

ANC method: MIMO feedforward FXLMS algorithm.

Case	Secondary source(s)	Error sensor(s)	Performance
1(a)	L_1	M_1	ATT_g = 0.42dB, ATT_1 = 5.18 dB
1(b)	L_4	M_4	ATT_g = 0.53dB, ATT_1 = 8.16 dB
2	L_4	M_3, M_4	ATT_g = 0.63dB, ATT_3 = -0.12 dB, ATT_4 = 7.53 dB
3(a)	L_1, L_2	M_1, M_2	ATT_g = 0.68 dB, ATT_1 = 3.96 dB, ATT_2 = 5.80 dB
3(b)	L_3, L_4	M_3, M_4	ATT_g = 1.86 dB, ATT_3 = 8.12 dB, ATT_4 = 7.31 dB
3(c)	L_3, L_4	M_1, M_2	ATT_g = -2.88 dB, ATT_1 = 1.89 dB, ATT_2 = 2.78 dB
4	L_1, L_3, L_4	M_1, M_3, M_4	ATT_g = 2.62dB, ATT_1 = 2.94 dB, ATT_2 = -0.02 dB ATT_3 = 8.10 dB, ATT_4 = 5.12 dB

Experiments were carried out to investigate the MIMO ANC techniques. The primary noise type, ANC algorithm, number of actuators and sensors, and the results for each test case are summarized in Tables 3 and 4. In part 1 of the experimental cases (Table 3), we first examine the effects of the position and number of actuators and sensors on the MIMO active control. A band-limited (0 ~ 400 Hz) random noise is used as the primary noise. The ANC method is the MIMO feedforward FXLMS algorithm. In Case 1(a), we use only one secondary source L_1 and one error sensor M_1. The total attenuation ATT_1 achieved at M_1 is 5.18 dB. In Case 1(b), we use L_4 as the actuator and M_4 as the error sensor. Maximum attenuation reaches 17 dB and ATT_4 is 0.53 dB. The results suggest that single actuator-sensor pair can provide local attenuation and the pair placed at the corner are more effective than those at the center of the wall. It is remarked that the references by Bai and Chang (1996), and by Molo and Bernhard (1989) seem to have different views from the reference by Cunefare and Koopman (1991) regarding the optimal allocation of sensors and actuators in active control: the first two references suggest placing sensors and actuators at the pressure maxima, while the last reference suggests placing sensors and actuators at the particle velocity maxima. Our experimental results appear to agree better with the conclusions in the first two references. In Case 2, we use one secondary source L_4 and two error sensors, M_3 and M_4. Attenuation is found only at the sensor M_4. In Case 3(a), we use two secondary sources L_1, L_2, and two error sensors M_1, and M_2. The total attenuation ATT_g is 0.68 dB after the ANC is activated. Case 3(b) shows the results when the collocated transducers L_3, L_4, M_3, and M_4 are used, where ATT_g is 1.86 dB, ATT_3 and ATT_4 are 8.12 dB and 7.31 dB, respectively. Case 3(c) shows the results when two noncollocated actuator-sensor pairs, L_3, L_4,

M_1, and M_2 are used. Although total attenuations of 1.89 dB and 2.78 dB in the band 50 ~ 400 Hz at M_1 and M_2 are obtained, the sound pressure is increased at M_3 and M_4. This amounts to an ATT_g of −2.88 dB. The results of this case suggest that collocated actuator-sensor pairs placed at the corners provide the largest noise cancellation. In Case 4, three collocated actuator-sensor pairs, $L_1 - M_1$, $L_3 - M_3$, and $L_4 - M_4$, are used. A total attenuation 2.62 dB of $\hat{E}_g(f)$ is obtained after the ANC is activated, which is the largest among the four cases.

From the above results in part I, the guidelines for locating of sensors and actuators in an ANC system can be summarized as follows. Collocated actuator-sensor pairs provide better performance than the non-collocated pairs. This is a well-known fact in structural control: that the transfer functions of collocated pairs have less non-minimal phase (NMP) zeros which impose design constraints on the control system (Miu, 1991). A sufficient number of sensors and actuators are needed for achieving global control. Furthermore, it is preferable to locate actuator-sensor pairs at the corners of the enclosure, where pressure maxima correspond to the best controllability and observability for the actuators and sensors.

Next, the performance of the MIMO ANC methods based on different control structures and algorithms are investigated. In all cases, L_3 and L_4 are used as the secondary sources, and M_3 and M_4 are used as the error sensors. The band-limited random noise is used as the primary noise. The results obtained from the feedforward FXLMS algorithm, the feedback FXLMS algorithm, the feedforward H_∞ algorithm, and the feedback H_∞ algorithm are compared in Cases 1 and 2. ATT_g for these four methods are 1.86 dB, 0.98 dB, 2.73 dB, and 0.24 dB, respectively. The results show that the feedforward structure is more effective than the feedback structure in suppressing broadband random noises. Among the ANC methods, the MIMO feedforward H_∞ algorithm produces the largest total reduction of $\hat{E}_g(f)$. The poles and zeros of the MIMO feedforward H_∞ controller are listed in Table 5.

Table 4 Experimental cases (Part 2). Multiple-channel ANC methods based on different control algorithms and structures are investigated.

Secondary sources: L_3, L_4 Error sensors: M_3, M_4			
Case	ANC method	Noise type	Performance
1	feedforward FXLMS	random noise	ATT_g = 1.86 dB, ATT_3 = 8.12 dB, ATT_4 = 7.31 dB
2(a)	feedback FXLMS	random noise	ATT_g = 0.98 dB, ATT_3 = 1.25 dB, ATT_4 = 2.11 dB
2(b)	feedforward H_∞	random noise	ATT_g = 2.73 dB, ATT_3 = 6.16 dB, ATT_4 = 5.17 dB
2(c)	feedback H_∞	random noise	ATT_g = 0.24 dB, ATT_3 = 0.59 dB, ATT_4 = 0.39 dB
3(a)	feedforward FXLMS	engine noise	ATT_g = 4.31 dB, ATT_3 = 11.20 dB, ATT_4 = 18.34 dB
3(b)	feedback FXLMS	engine noise	ATT_g = 3.73 dB, ATT_3 = 11.33 dB, ATT_4 = 20.76 dB
3(c)	feedforward H_∞	engine noise	ATT_g = 5.08 dB, ATT_3 = 11.24 dB, ATT_4 = 7.86 dB
3(d)	feedback H_∞	engine noise	ATT_g = 3.14 dB, ATT_3 = 6.21 dB, ATT_4 = 5.84 dB

Table 5 A list of poles and zeros of the feedforward H_∞ controller, where C stands for the controller; the subsripts 3 and 4 stand for the corresponding speaker numbers.

$C_3(z)$		$C_4(z)$	
zeros	poles	zeros	poles
-0.9367	-0.9595	32.6950	-0.9730
-0.7504	-0.9549	-0.8905	-0.8442
-0.3649±0.4738i	-0.5189	1.7224	-0.5789
1.5051	0.4243±0.8280i	-0.4437±0.5089i	0.2091±0.8316i
0.3248±0.7475i	0.0540±0.3399i	0.2622±0.6099i	0.0477±0.3749i
0.2846±0.4718i	0.7498±0.6016i	0.2672±0.5344i	0.7018±0.7008i
0.7995±0.6486i	0.7840±0.5599i	0.7440±0.7157i	0.7545±0.6463i
0.7944±0.5692i	0.8172±0.5384i	0.7519±0.6616i	0.8358±0.5442i
0.8056±0.5178i	0.8731±0.4111i	0.8359±0.5422i	0.8244±0.5323i
0.9410±0.2764i	0.9509±0.2853i	0.8219±0.5409i	0.8115±0.4928i
0.9153±0.1683i	0.9714±0.1232i	0.8097±0.4387i	0.8914±0.4166i
0.9203±0.0913i	0.9551±0.0303i	0.9527±0.2552i	0.9558±0.2768i
0.8206	0.8725	0.9842±0.1282i	0.9825±0.1270i
0.4317	0.3552	0.9247±0.1002i	0.9540±0.1113i
-0.0898	-0.1075	0.8426±0.2205i	0.9739±0.0634i
		0.5154±0.0978i	0.4272±0.0113i
		-0.1151	-0.1088
gain = -1.93E-2		gain = 8.9319E-4	

Next, in Case 3, exhaust noise from the gasoline engine operating at 4,000 rpm is chosen as a more practical primary noise. The ATT_g obtained by using the feedforward FXLMS algorithm, the feedback FXLMS algorithm, the feedforward H_∞ algorithm, and the feedback H_∞ algorithm are 4.31 dB, 3.73 dB, 5.08 dB, and 3.14 dB, respectively. The feedforward H_∞ algorithm again yields the largest global attenuation of $\hat{E}_g(f)$.

Concluding Remarks

Multiple-channel ANC systems based on the FXLMS algorithm and the H_∞ algorithm are investigated. Both feedforward and feedback ANC structures are investigated. Experiments are carried out to compare the ANC approaches for attenuation of the internal field in an enclosure. Number and position of actuators and sensors required to achieve global control is also examined.

Insofar as the allocation of sensors and actuators is concerned, a useful strategy is to place a sufficient number of collocated actuator-sensor pairs to create connected quiet zones distributed in the enclosure. In particular, it is preferred to place the actuator-sensor pairs in the regions of pressure maxima.

All ANC algorithms yield significant noise reductions for periodic (engine) noises. For a high-order plant such as the enclosure in our case, the feedforward structure appears to be a more viable approach for broadband cancellation. The feedback structure suffers from the waterbed effect and only narrowband noise rejection can be achieved. The adaptive methods and the H_∞ methods exhibit comparable performance for both random noise and engine noise irrespective of the control structure. However, only the MIMO feedforward H_∞ technique is effective in suppressing transient noises.

One important issue that is not addressed in this paper is the acoustic feedback problem associated with the feedforward structure. In some practical situations, only acoustical reference signals sensed by upstream microphones are available so that one is faced with the problem of acoustic feedback. This will considerably complicate the MIMO control design from the standpoint of performance and robustness. The future investigations will focus on this particular aspect.

Acknowledgment

The work was supported by the National Science Council in Taiwan, Republic of China, under the project number NSC 86-2212-E-009-003.

References

Bai, M. R., and Chang, S., 1996, "Active Noise Control of Enclosed Harmonic Fields by Using BEM-Based Optimization Techniques," *Applied Acoustics*, Vol. 48, No. 1, pp. 15–32.

Cunefare, K. A., and Koopman, G. H., 1991, "A Boundary Element Approach to Optimization of Active Noise Control Sources on Three-Dimensional Structures," ASME, JOURNAL OF VIBRATION AND ACOUSTICS, Vol. 113, pp. 387–394.

Doyle, J. C., Francis, B. A., and Tannenbaum, A. R., 1992, *Feedback Control Theory,* Macmillan Publishing Company, New York.

Doyle, J. C., Glover, K., Khargonekar, P., and Francis, B. A., 1989, "State Space Solution to Standard H_2 and H_∞ Control Problems," *IEEE Trans. on Automatic Control,* Vol. AC-34, No. 8, pp. 832–847.

Elliott, S. J., and Nelson, P. A., 1994, "Active Noise Control," *Noise/News International,* Vol. 2, No. 2, pp. 75–98.

Elliott, S. J., Boucher, C. C., and Nelson, P. A., 1992, "The Behavior of a Multiple Channel Active Control System," *IEEE Transactions on Signal Processing,* Vol. 40, No. 5, pp. 1041–1052.

Elliott, S. J., Nelson, P. A., Stothers, I. M., and Boucher, C. C., 1990, "In-Flight Experiments on the Active Control of Propeller-Induced Cabin Noise," *Journal of Sound and Vibration,* Vol. 140, pp. 219–238.

Elliott, S. J., Stothers, I. M., and Nelson, P. A., 1987, "A Multiple Error LMS Algorithm and Its Application to the Active Control of Sound and Vibration," *IEEE Transactions on Acoustics, Speech, and Signal Processing,* Vol. ASSP-35, No. 10, pp. 1423–1434.

Fuller, C. R., and Von Flotow, A. H., 1995, "Active Control of Sound and Vibration," *IEEE Control Systems Magazine,* Vol. 2, pp. 9–19.

Iglesias, P. A., and Glover, K., 1991, "State-Space Approach to Discrete-Time H_∞ Control," *International Journal of Control,* Vol. 54, pp. 1031–1072.

Kinsler, L. E., Frey, A. R., Coppens, A. B., and Sanders, J. V., 1982, *Fundamentals of Acoustics,* 3rd Ed., John Wiley and Sons, New York.

Kuo, S. M., and Morgan, D. R., 1996, *Active Noise Control Systems,* John Wiley and Sons, New York.

Lester, H. C., and Fuller, C. R., 1990, "Active Control of Propeller-Induced Noise Fields inside a Flexible Cylinder," *AIAA Journal,* Vol. 28, No. 8, pp. 1374–1380.

Lin, C. F., 1994, *Advanced Control Systems Design,* Prentice-Hall, Englewood Cliffs.

Ljung, L., 1987, *System Identification: Theory for the User,* Prentice-Hall, Englewood Cliffs.

McFarlane, D. C., and Glover, K., 1989, *Robust Controller Design Using Normalized Coprime Factor Plant Design,* Springer-Verlag, Berlin.

Miu, D. K., 1991, "Physical Interpretation of Transfer Function Zeros for Simple Control Systems with Mechanical Flexibilities," ASME *Journal of Dynamic Systems, Measurement, and Control,* Vol. 113, pp. 419–424.

Molo, C. G., and Bernhard, R. J., 1989, "Generalized Method of Predicting Optimal Performance of Active Noise Controllers," *AIAA Journal,* Vol. 27, No. 11, pp. 1473–1478.

Nelson, P. A., and Elliott, S. J., 1992, *Active Control of Sound,* Academic Press, San Diego.

Snyder, S. D., and Hansen, C. H., 1992, "Design Considerations for Active Noise Control Systems Implementing the Multiple Input, Multiple Output LMS Algorithm," *Journal of Sound and Vibration,* Vol. 159, pp. 157–174.

Tsai, M. C., and Tsai, C. S., 1995, "A Transfer Matrix Framework Approach to the Synthesis of H_∞ Controllers," *International Journal of Control,* Vol. 5, pp. 155–173.

Yeh, F. B., and Yang, C. D., 1992, *Post Modern Control Theory and Design,* Eurasia, Taipei, Taiwan.

Youla, D. C., Jabr, H. A., and Bongiorno, J. J., 1976, "Modern Wiener-Hopf Design of Optimal Controllers, Part 2: the Multivariable Case," *IEEE Trans. Auto. Control,* Vol. 21, pp. 319–338.